The highly stable air-working electro-active ionic polymer actuator based on nitrogen-doped graphene aerogel flexible electrode

Kai Xiang[1], Tian Chen[1,*] , and Yanni Wang[1]

[1] College of Materials Science and Technology, Nanjing University of Aeronautics and Astronautics, Nanjing 210016, China

ABSTRACT

Three-dimensional nitrogen-doped graphene aerogels (3D N-GAs) were prepared by ultrasonic stripping, hydrothermal reduction and freeze drying. Those N-GAs exhibited high-specific surface area, high nitrogen doping amount, and 3D porous network structure. Soft electro-active ionic polymer actuators were developed for the first time using this 3D N-GA soft electrode. The developed soft actuator exhibited large peak-to-peak displacement of 11.8 mm (3 V and 0.1 Hz) and high air working durability for 93.8% after 6 h cycles. These successful demonstrations elucidated the wide potential of 3D N-GA soft actuators for the next-generation soft robotic devices.

1 Introduction

Electro-active polymer (EAP) actuators have received great interest as artificial muscles for use in soft robotics, wearable touch-feedback systems, stretchable and flexible electronics, and microelectromechanical systems (MEMS) [1, 2]. EAP actuators can be divided into two categories according to the working mechanism, that is, electro-active electronic polymer (EAEP) actuators and electro-active ionic polymer (EAIP) actuators [3]. EAEPs consist of materials such as electrostrictive elastomers [4], ferroelectric polymers [5], and dielectric elastomers [6]. EAIPs consist of materials such as polymer gels [7], conducting polymers [8], and ionic polymer-metal composites (IPMC) [9]. In the area of soft EAIP actuators, IPMC actuators arise as one of the most suitable options to develop low cost, and low weight devices, as they allow low operating applied potential difference and large deformations [10–21].

Traditional IPMC is composed of an ion exchangeable polymer and noble metal electrodes [22]. Recently, several carbon materials have been explored as flexible electrode for new IPMC actuators. Among carbon materials, graphene is of particular interest because of its one-atom-thick carbon layer with sp^2-hybridized bonds, which has exceptional mechanical and electrical properties [23]. Chen et al. and Oh et al. developed soft ionic actuators using different graphene hybrid electrodes [13, 24–26]. Although a number of graphene-based electrode IPMC actuators have been developed, graphene aerogel and nitrogen-doped graphene aerogel

Address correspondence to E-mail: chentian@nuaa.edu.cn

has not been investigated as an efficient electrode for highly bendable IPMC actuator so far.

Graphene aerogel is a novel graphene material in which individual graphene sheets are bonded together to construct three-dimensional porous networks [27]. Graphene aerogels are usually produced using sol–gel chemistry, which involves reducing graphene oxide to form a highly cross-linked graphene hydrogel, followed by freeze-drying to remove the absorbed water [28]. Like other nitrogen-doped carbon materials, nitrogen-doped graphene aerogels can be obtained by introducing a nitrogen source into the preparation process of graphene aerogels. Nitrogen atom doping in graphene creates charged sites and results in redistribution of spin and charge densities in graphene by disrupting the ideal sp^2 hybridization of carbon atoms, improving the conductivity and providing more active sites for electrochemical reactions [29].

In this study, novel EAIP actuators were prepared using nitrogen-doped graphene aerogels. In addition, by changing the ratio of raw materials, we obtained a series of 3D N-GAs with different nitrogen content. The effect of nitrogen content on actuating performance was investigated in detail. We further investigated the influence of 3D N-GA electrode material amount on the actuating performance of the actuator. To the best of our knowledge, this type of 3D N-GA actuator has not been reported.

2 Experimental

2.1 Chemicals

Graphite oxide was supplied by Nanjing XF Nano co., Ltd. Urea was supplied by Sinopharm Chemical Reagent Co.,Ltd. PEDOT:PSS (1.05 wt%) was supplied by Shanghai Ouyi organic photoelectric material co., Ltd. 1-ethyl-3-methylimidazolium tetrafluoroborate ($EMIBF_4$) was commercially available from Aladin chemical co., Ltd. PVDF-HFP was commercially available from shanghai 3F co., Ltd.

2.2 Preparation of nitrogen-doped graphene aerogels

Graphite oxide was placed in an ultrasonic cleaning machine for 48 h ultrasonic treatment. Graphite oxide was stripped by ultrasonic. Then we got graphene oxide (GO) solution. After drying the GO solution we got the GO powder. Different concentration of GO/urea solution was prepared by adding certain amount of GO powder and urea powder into water. The ratio of GO and urea was 3:1, 2:1, 1:1, and 1:5. After that GO/urea solution was placed in a hydrothermal reactor. GO/urea solution was hydrothermal treated at 180 °C for 12 h. Then we got nitrogen-doped graphene hydrogel. Finally nitrogen-doped graphene aerogels were obtained by freeze drying the graphene hydrogel at − 50 °C for 48 h. The graphene aerogel was prepared for comparisons by the same method just without adding the urea. The synthetic route of nitrogen-doped graphene aerogel is shown in Fig. 1.

2.3 Preparation of EAIP actuator

PVDF-HFP/IL electrolyte layer was prepared to direct the cast of the PVDF-HFP/IL solution in a glass mold. The sample was then dried at 80 °C for 30 min.

Nitrogen-doped graphene aerogel/PEDOT:PSS flexible electrode was prepared to direct the cast of the nitrogen-doped graphene aerogel/PEDOT:PSS solution in a glass mold and then dried in a vacuum drying box at 60 °C.

The EAIP actuator was prepared by hot-pressing at 90 °C for 5 min with two layers of nitrogen-doped graphene aerogel/PEDOT:PSS electrode film and one layer of PVDF-HFP/$EMIBF_4$ electrolyte layer.

2.4 Characterization

The structures of N-GAs were analyzed by X-ray diffraction (XRD) (Bruker D8 Advance diffractometer). The surface morphologies of the N-GAs were observed by scanning electron microscope (SEM) (FEI Nova nano 450). Brunauer–Emmett–Teller (BET) measurements were performed with N_2 adsorption/desorption isotherms instrument (Micromeritics ASAP 2020). The chemical composition of the N-GAs was analyzed using X-ray photoelectron spectroscopy (Thermo ESCALAB250Xi spectrometer). The electric-induced displacement of the EAIP actuator was measured by a laser positioning system (Keyence LK-G80). For displacement measurement, the actuator size was made to 25 mm*5 mm. The strain (ε) of the actuator was estimated by the following equation [2, 14]:

Fig. 1 The synthetic route of nitrogen-doped graphene aerogel
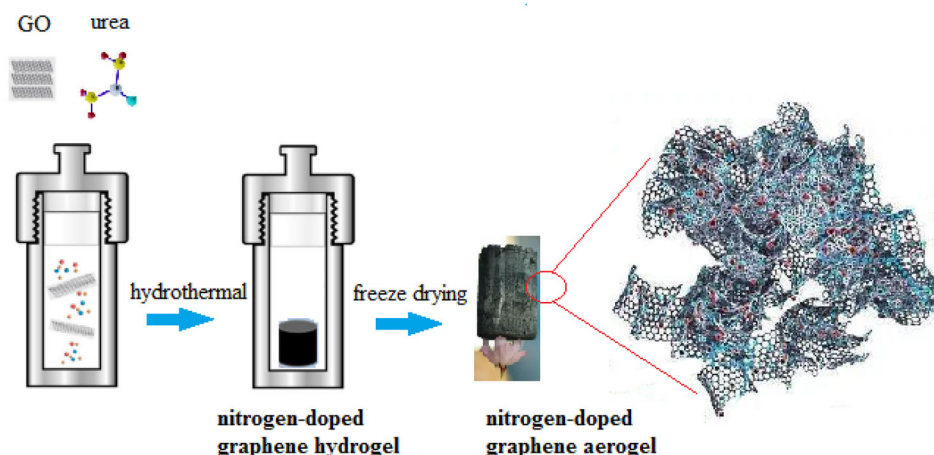
$$\varepsilon = \frac{2d\delta}{\delta^2 + L^2}$$

where d, δ and L are the thickness, tip displacement and free length of the actuator strip, respectively.

3 Results and discussion

XRD patterns of GO and 3D N-GA(x) are shown in Fig. 2. The peak at 11° for GO corresponds to the (001) crystal plane with a d-spacing of 0.86 nm. After the hydrothermal reduction of GO, wide diffraction peaks appeared at 25.2° for 3D N-GA(x). The d-spacing of 3D N-GA(x) is 0.35 nm. The decrease d-spacing showed that the reduction of GO eliminates the functional groups such as the epoxy groups. The presence of a broad band at 25.2° was also attributed

to the irregular structure of the GA and the random overlapping of the graphene sheets to form irregular network of pores [30].

XPS tests of 3D N-GA(x) are shown in Figs. 3 and 4. Figure 3 shows XPS survey spectra of 3D N-GA(x). They exhibited typical N1s peaks along with C1s and O1s, which indicated the successful doping of N atoms inside the GA lattice. Figure 4a–h show C1s and N1s XPS spectra of different 3D N-GA(x). The C1s peaks can be fitted to five typical peaks at 284.8, 285.9, 286.9, 288.7 and 291.3 eV, corresponding to C-C, C-O, C-N, O-C=O and C=C, respectively [31]. In addition, the nitrogen-containing groups in the 3D N-GA(x) samples were confirmed by the high-resolution N1s spectra. The three characteristic peaks at 398.2, 399.7 and 401.9 eV correspond to pyridinic, pyrrolic and graphitic nitrogen in 3D N-GA(x). From the XPS data we also get the N1s atomic% of different
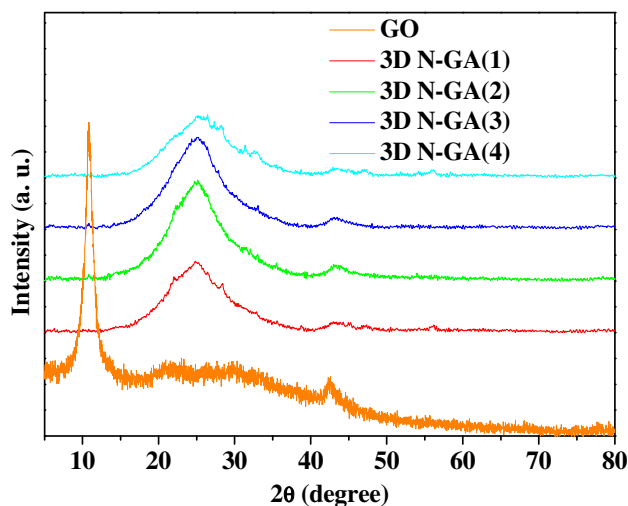

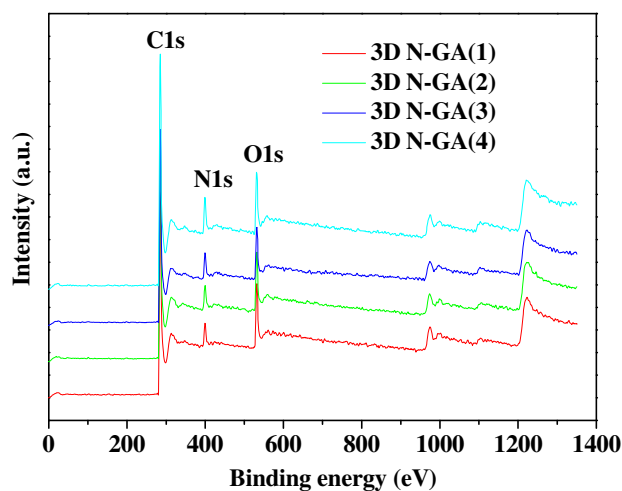
Fig. 2 XRD patterns of GO and different 3D N-GA(x)

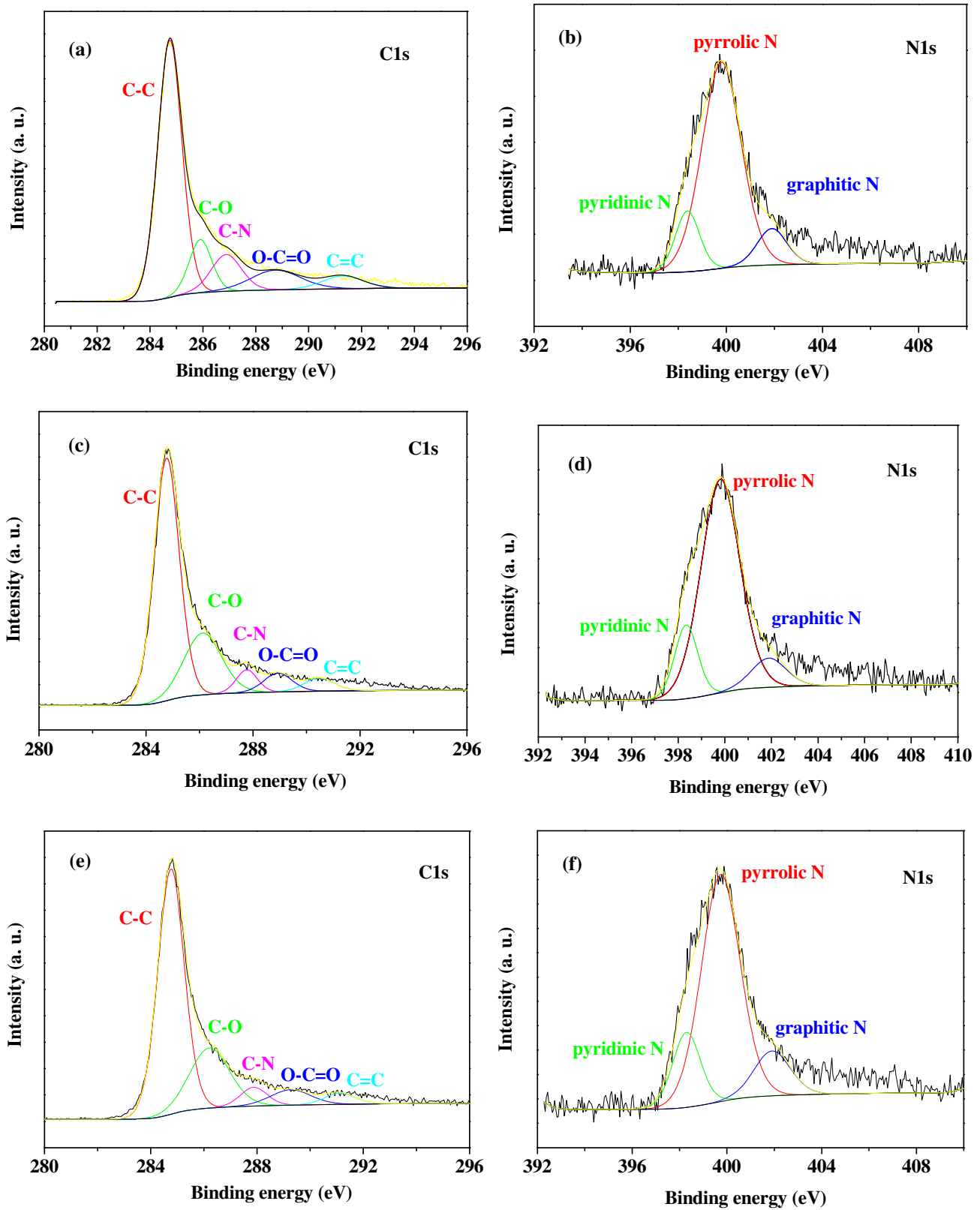
Fig. 3 XPS survey spectra of 3D N-GA(x)

Fig. 4 **a** C1s and **b** N1s XPS spectrum of 3D N-GA(1). **c** C1s and **d** N1s XPS spectrum of 3D N-GA(2). **e** C1s and **f** N1s XPS spectrum of 3D N-GA(3). **g** C1s and **h** N1s XPS spectrum of 3D N-GA(1)
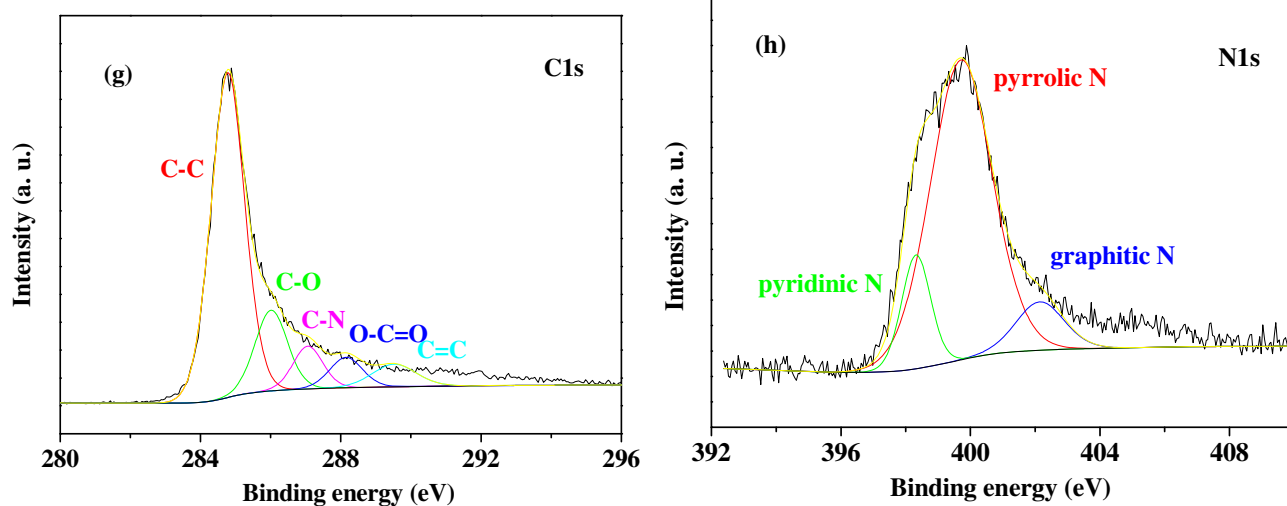
Fig. 4 continued

3D N-GA(x), as shown in Table 1. The N1s atomic% of 3D N-GA(1), (2), (3) and (4) was 6.57, 7.29, 8.31 and 8.89.

Figure 5 demonstrates the SEM images of the 3D N-GA(x). The 3D N-GA(x) showed the obvious three dimensional porous networks with abundant voids. There is π–π interaction between the graphene sheets forming the three-dimensional graphene pore structure, and there is electrostatic repulsion between the oxygen-containing functional groups on the sheets. The balance of these two forces ensured the stable existence of the three-dimensional graphene aerogel pore structure. The morphology of 3D N-GA(1), (2), (3) and (4) was nearly the same.

To investigate the specific surface area and porosity of 3D N-GA, we measured the N_2 adsorption–desorption isotherm and the pore-size distribution curves. As shown in Fig. 6a, the N_2 adsorption–desorption curves follow a type IV isotherm curve according to the IUPAC classification, which is characteristic of a mesoporous material [32]. The specific surface area, pore volume and the average porous size of 3D N-GA(1), (2), (3) and (4) are summarized in Table 2. 3D N-GA(2) has the highest specific surface area among four 3D N-GAs. The specific surface area and pore volume of 3D N-GA(2) was 127.33 m^2/g and 0.2263 cm^3/g. The specific surface area of 3D N-GA(3) was 104.88 m^2/g and the specific surface area of the other graphene aerogels was below 100 m^2/g.

The soft EAIP actuator with sandwich structure was prepared by hot-pressing. Figure 7 shows the

Table 1 Comparisons of different XPS results of the tested N-doped graphene aerogel

Sample	C1s atomic%	O1s atomic%	N1s atomic%
3D N-GA(1)	83.04	10.39	6.57
3D N-GA(2)	83.08	9.63	7.29
3D N-GA(3)	82.39	9.3	8.31
3D N-GA(4)	82.17	8.95	8.89

schematic diagram for EAIP actuator with novel 3D N-GA electrodes. Figure 7 also displays the cross-sectional SEM picture of our EAIP actuator with novel 3D N-GA electrodes. From the SEM we could clearly see the electrode/electrolyte/electrode sandwiched structure. There was no obvious interfacial gap between the electrode layer and the electrolyte layer. Our EAIP actuator is nearly 100 μm.

We investigated the actuation performances of the EAIP actuators in detail. First of all, we compared the displacement performances of four 3D N-GA(x) actuators and 3D GA actuator under the condition of the same electrode material amount (1 mg) (Fig. 8). 3D N-GA actuators displayed obviously better performance than that of 3D GA actuator. 3D N-GA(3) actuator showed the best actuating performance among the four 3D N-GA actuators. The order of the actuating performance of EAIP actuators was: 3D N-GA(3) > 3D N-GA(2) > 3D N-GA(1) > 3D N-GA(4). The peak-to-peak displacement of 3D N-GA(3) was 11.1 mm under 3 V at 0.1 Hz. The good performance of the 3D N-GA(3) actuator was
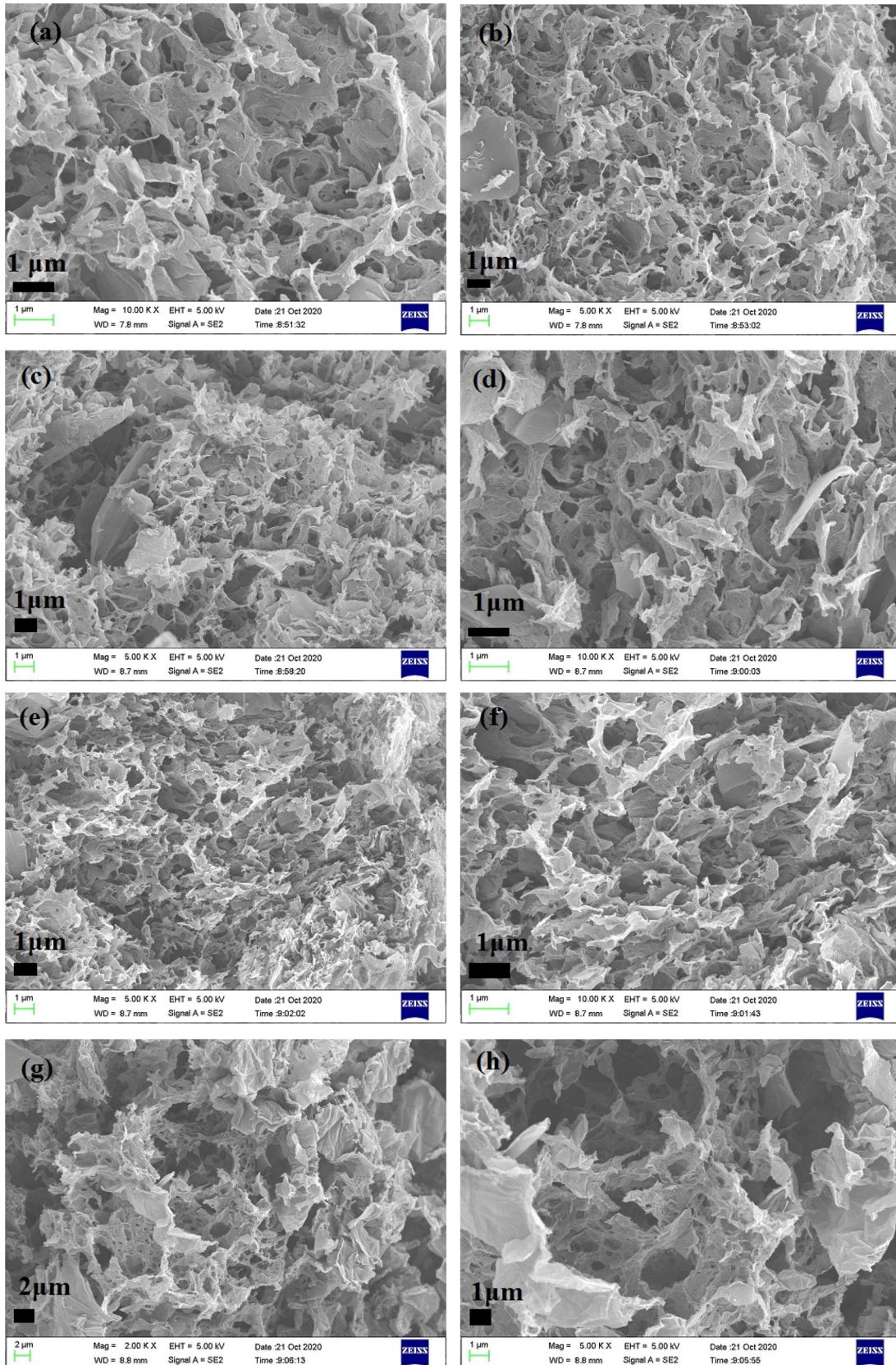
◄ **Fig. 5** **a**, **b** SEM images of 3D N-GA(1). **c**, **d** SEM images of 3D N-GA(2). **e**, **f** SEM images of 3D N-GA(3). **g**, **h** SEM images of 3D N-GA(41)

attributed to the large nitrogen doping amount (8.31 atomic%) and the large specific surface area (104.88 m²/g) of 3D N-GA(3).

As to 3D N-GA(3) actuator, we further investigated the influence of electrode material amount on the actuating performance of the actuator. With the increase of 3D N-GA electrode material weight, the actuating performance of the actuator increased first and then decreased, as shown in Fig. 9. When the electrode material dosage is 2 mg, the actuating performance of the 3D N-GA(3) actuator is the best (11.8 mm under 3 V at 0.1 Hz). Figure 10 shows the electric-induced displacement curves of the different 3D N-GA(3) actuators under input voltages of 1.0, 2.0, and 3.0 V at 0.1 Hz. The electric-induced displacement increased linearly. The law of almost linear growth was in accordance with other reports [25]. The 3D N-GA(3) (2 mg) actuator showed larger electric-induced displacement than the other actuators.
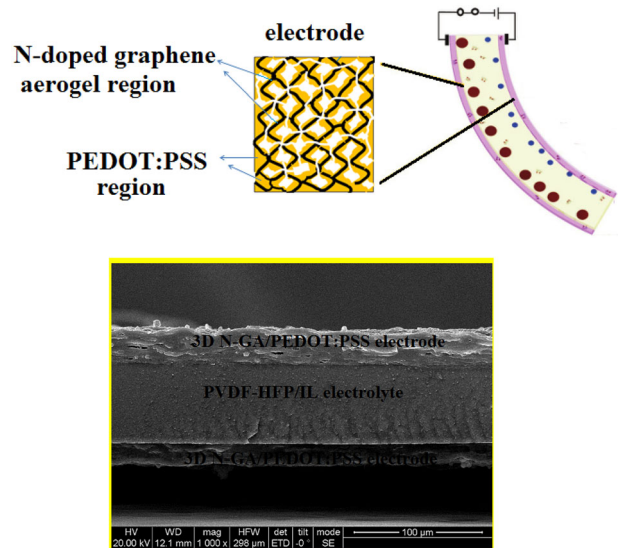

Fig. 7 Schematic diagram and cross-sectional SEM picture for electro-active ionic polymer actuator with 3D N-GA electrodes

The electric-induced displacement curves of the 3D N-GA(3) actuator at different frequencies (0.1, 0.5 and 1.0 Hz) are displayed in Fig. 11. As the frequency increased, the electric-induced displacement obviously decreased. This is because the higher was the
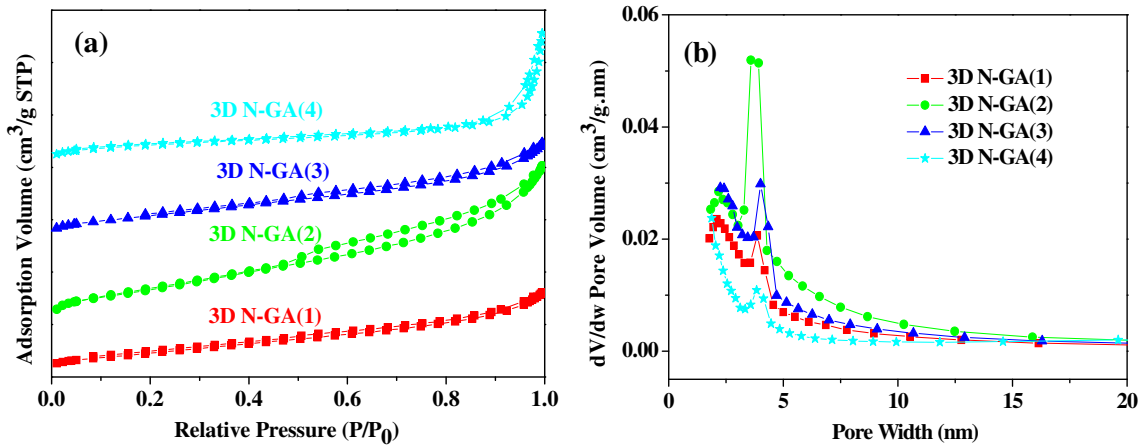

Fig. 6 **a** N_2 adsorption–desorption isotherms and **b** corresponding pore-size distributions of 3D N-GA(x)

Table 2 BET characterization results of 3D N-GA(x)

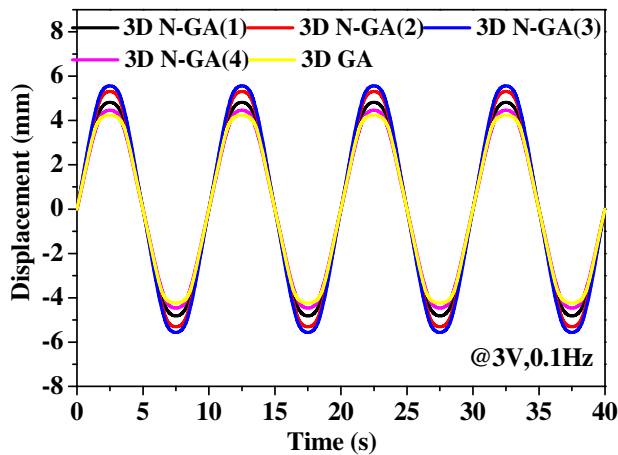| Sample	BET surface area (m²/g)	Pore volume (cm³/g)	Pore size (nm)
3D N-GA(1)	83.4969	0.126730	5.0789
3D N-GA(2)	127.3366	0.226264	5.6264
3D N-GA(3)	104.8848	0.150736	5.8032
3D N-GA(4)	74.1698	0.098779	6.2669

Fig. 8 The electric-induced displacement curves of different 3D N-GA(*x*) and 3D GA actuators under 3 V at 0.1 Hz

frequency; the shorter was the time available for ion migration. This rule was in accordance with other reports [20, 33]. Figure 12 shows the bending strain of the 3D N-GA(3) actuator at different frequencies. The bending strain of 3D N-GA(3) actuator was 0.47% at 0.1 Hz (3.0 V). Table 3 compares the bending strains of some EAIP actuators. 3D N-GA(3) actuator displayed good performance.

Cyclic stability is an important parameter to evaluate the performance of actuator. We measured the cyclic stability performance of the 3D N-GA(3) actuator. Figure 13 shows the actuating stability data for the 3D N-GA(3) actuator over a long period of 6 h. From the actuating stability figure we could clearly see that there was not any obvious performance degradation for 3D N-GA(3) actuator after 6 h
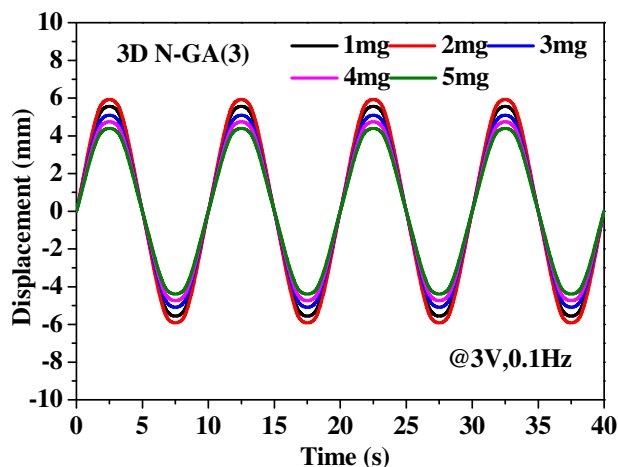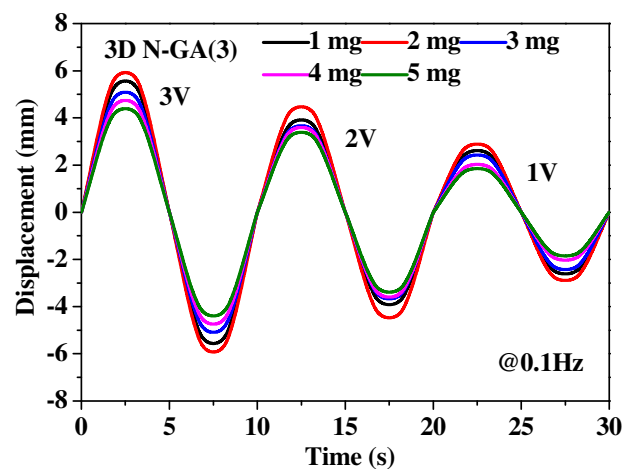

Fig. 10 The electric-induced displacements of different 3D N-GA(3) actuators under varying input voltages (1–3 V) at 0.1 Hz
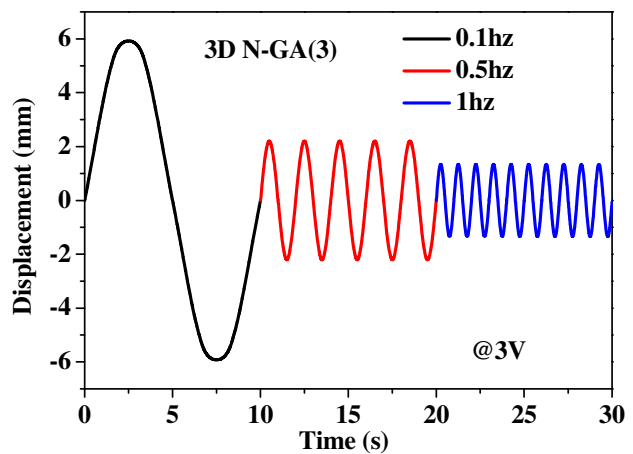

Fig. 11 The electric-induced displacements of the 3D N-GA(3) actuator under 3 V sine wave input voltage at different frequencies (0.1–1 Hz)
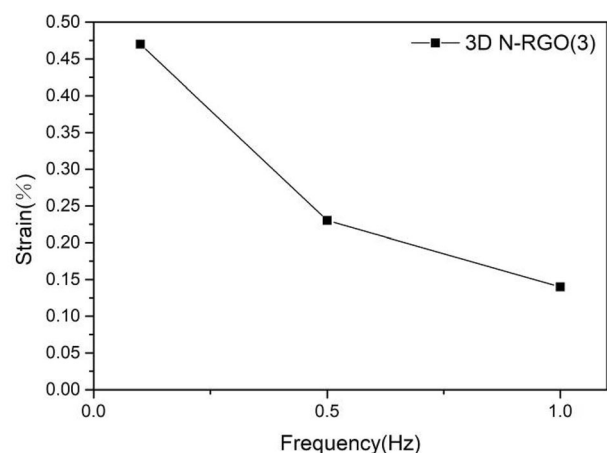

Fig. 9 The electric-induced displacement curves of different 3D N-GA(3) actuators under 3 V at 0.1 Hz

Fig. 12 Actuating strain of the 3D N-GA(3) actuator under 3 V sine wave input voltage at different frequencies (0.1–1 Hz)

Table 3 Bending strains of the 3D N-GA(3) actuator in comparison with that of other EAIP actuators reported in the literatures

Reference	Electrode	Polymer matrix	Ionic liquid	Bending strain	Voltage (V)	Frequency (Hz)
This study	3D nitrogen-doped graphene aerogel	PVDF-HFP	EMIBF$_4$	0.47%	3.0	0.1
[14]	Graphdiyne	PVDF	EMIBF$_4$	0.07%	2.5	30
[16]	Conductive graphite	PVDF	EMIBF$_4$	11.1 mm	10	0.1
[20]	Black-phosphorous	PVDF-HFP	EMIBF$_4$	1.67% (peak-to-peak)	2.5	0.1
[24]	Graphene nanosheet/carbon nanotube	PVDF	EMIBF$_4$	3.8 mm	2	0.1
[33]	Nacre-based carbon nanomesh	PVDF	EMIBF$_4$	1.11%	3	0.1
[34]	Graphene-Ag	PVDF	EMIBF$_4$	1.5 mm	1	0.1
[35]	Vapor-grown carbon fibre	PVDF-HFP	EMIBF$_4$	0.79%	2	0.1
[36]	Au	PVDF	PMITFSI	0.35%	5	0.1
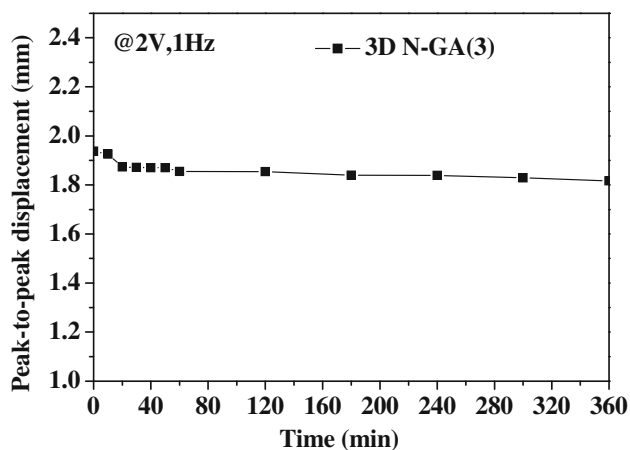
Fig. 13 Durability result (6 h) of peak-to-peak displacements for the 3D N-GA(3) actuator under 2 V at 1 Hz

actuating operation (2 V, 1 Hz). After 6 h test, the displacement of the 3D N-GA(3) actuator decreased from the initial 1.94–1.82 mm, maintaining a relative initial bending displacement of 93.8%. These results demonstrated the good air-working stability of this novel 3D N-GA(3) actuator based on nitrogen-doped graphene aerogel soft electrode.

4 Conclusions

In summary, soft EAIP actuators were developed for the first time using a novel 3D nitrogen-doped graphene aerogel soft electrode. In this study, we investigated the influence of nitrogen doping amount and electrode material amount on actuating performance of 3D N-GA actuators. 3D N-GA(3) has relatively high nitrogen content and relatively large specific surface area and 3D N-GA(3) actuator has the best actuating performance. Furthermore, with the increase of electrode material consumption, the actuating performance of the 3D N-GA(3) actuator increased first and then decreased. When the electrode material dosage is 2 mg, the actuating performance of the 3D N-GA(3) actuator is the best (11.8 mm under 3 V at 0.1 Hz). The 3D N-GA actuator exhibited high actuation performances, e.g. low actuating voltage below 3 V, large electric induced displacement of 11.8 mm, and 6 h cycles air working durability. Thus, this 3D N-GA actuator will have great potential application in soft robotics and smart devices.

References

1. D. Chen, Q.B. Pei, Electronic muscles and skins: a review of soft sensors and actuators. Chem. Rev. **117**, 11239–11268 (2017)

2. S. Umrao, R. Tabassian, J.W. Kim, V.H. Nguyen, Q.T. Zhou et al., Mxene artificial muscles based on ionically cross-linked $Ti_3C_2T_x$ electrode for kinetic soft robotics. Sci. Robot. **4**, 17797 (2019)

3. L.R. Kong, W. Chen, Carbon nanotube and graphene-based bioinspired electrochemical actuators. Adv. Mater. **26**, 1025–1043 (2014)

4. Y. Wang, C. Sun, E. Zhou, J. Su, Deformation mechanisms of electrostrictive graft elastomer. Smart Mater. Struct. **13**, 1407 (2004)

5. Q.M. Zhang, V. Bharti, X. Zhao, Giant electrostriction relaxorferroelectric behavior electron-irradiated poly (vinylidene fluoride-trifluoroethylene) copolymer. Science **280**, 2101–2104 (1998)

6. L.J. Romasanta, M.A. Lopez-Manchado, R. Verdejo, Increasing the performance of dielectric elastomer actuators: a review from the materials perspective. Prog. Polym. Sci. **51**, 188–211 (2015)

7. Y. Osada, H. Okuzaki, H. Hori, A polymer gel with electrically driven motility. Nature **355**, 242–244 (1992)

8. T.F. Otero, J.G. Martinez, Physical and chemical awareness from sensing polymeric artificial muscles. Experiments and modeling. Prog. Polym. Sci. **44**, 62–78 (2015)

9. C. Jo, D. Pugal, I.K. Oh, K.J. Kim, K. Asaka, Recent advances in ionic polymer-metal composite actuators and their modeling and applications. Prog. Polym. Sci. **38**, 1037–1066 (2013)

10. J.C. Dias, D.M. Correia, C.M. Costa, C. Ribeiro, A. Maceiras, J.L. Vilas et al., Improved response of ionic liquid-based bending actuators by tailored interaction with the polar fluorinated polymer matrix. Electrochim. Acta **296**, 598–607 (2019)

11. A. Punning, K.J. Kim, V. Palmre, F. Vidal, C. Plesse, N. Festin et al., Ionic electroactive polymer artificial muscles in space applications. Sci. Rep. **4**, 6913 (2014)

12. N. Terasawa, K. Asaka, High-performance graphene oxide/vapor-grown carbon fiber composite polymer actuator. Sens. Actuators B **255**, 2829–2837 (2018)

13. M. Kotal, J. Kim, K.J. Kim, I.K. Oh, Sulfur and nitrogen Co-doped graphene electrodes for high-performance ionic artificial muscles. Adv. Mater. **28**, 1610–1615 (2016)

14. C. Lu, Y. Yang, J. Wang, R.P. Fu, X.X. Zhao, L. Zhao et al., High-performance graphdiyne-based electrochemical actuators. Nat. Commun. **9**, 752 (2018)

15. Q.S. He, M. Yu, X. Yang, K.J. Kim, Z.D. Dai, An ionic electro-active actuator made with graphene film electrode, chitosan and ionic liquid. Smart Mater. Struct. **24**, 065026 (2015)

16. D.J. Guo, Y.B. Han, J.J. Huang, E.C. Meng, L. Ma, H. Zhang et al., Hydrophilic poly(vinylidene fluoride) film with

enhanced inner channels for both water- and ionic liquid-driven ion-exchange polymer metal composite actuators. ACS Appl. Mater. Interfaces **11**, 2386–2397 (2019)

17. H.S. Wang, J. Cho, D.S. Song, J.H. Jang, J.Y. Jho, J.H. Park, High-performance electroactive polymer actuators based on ultra-thick ionic polymer-metal composites with nanodispersed metal electrodes. ACS Appl. Mater. Interfaces **9**, 21998–22005 (2017)

18. K. Bian, H. Liu, G. Tai, K.J. Zhu, K. Xiong, Enhanced actuation response of Nafion-based ionic polymer metal composites by doping $BaTiO_3$ nanoparticles. J. Phys. Chem. C **120**, 12377–12384 (2016)

19. L.F. Chang, H.L. Chen, Z.C. Zhu, B. Li, Manufacturing process and electrode properties of palladium-electroded IPMC. Smart Mater. Struct. **21**, 065018 (2012)

20. G. Wu, X.J. Wu, Y.J. Xu, H.Y. Cheng, J.K. Meng, Q. Yu et al., High-performance hierarchical black-phosphorous-based soft electrochemical actuators in bioinspired applications. Adv. Mater. **31**, 1806492 (2019)

21. F.Z. Lu, K. Xiang, Y.N. Wang, T. Chen, Electrochemical actuators based on nitrogen-doped carbons derived from zeolitic imidazolate frameworks. Mater. Design **187**, 108405 (2020)

22. M. Shahinpoor, K.J. Kim, Ionic polymer-metal composites: I. Fundamentals. Smart Mater. Struct. **10**, 819–833 (2001)

23. J. Kim, J.H. Jeon, H.J. Kim, H. Lim, I.K. Oh, Durable and water-floatable ionic polymer actuator with hydrophobic and asymmetrically laser-scribed reduced graphene oxide paper electrodes. ACS Nano **8**, 2986–2997 (2014)

24. L.H. Lu, J.H. Liu, Y. Hu, Y.W. Zhang, H. Randriamahazaka, W. Chen, Highly stable air working bimorph actuator based on a graphene nanosheet/carbon nanotube hybrid electrode. Adv. Mater. **24**, 4317–4321 (2012)

25. M. Kotal, J. Kim, R. Tabassian, S. Roy, V.H. Nguyen, N. Koratkar et al., Highly bendable ionic soft actuator based on nitrogen-enriched 3D hetero-nanostructure electrode. Adv. Funct. Mater. **28**, 1802464 (2018)

26. R. Tabassian, J. Kim, V.H. Nguyen, M. Kotal, I.K. Oh, Functionally antagonistic hybrid electrode with hollow tubular graphene mesh and nitrogen-doped crumpled graphene for high-performance ionic soft actuators. Adv. Funct. Mater. **28**, 1705714 (2018)

27. Y.F. Ma, Y.S. Chen, Three-dimensional graphene networks: synthesis, properties and applications. Natl. Sci. Rev. **2**, 40–53 (2015)

28. M.A. Worsley, P.J. Pauzauskie, T.Y. Olson et al., Synthesis of graphene aerogel with high electrical conductivity. J. Am. Chem. Soc. **132**, 14067–14069 (2010)

29. G. Wu, Y. Hu, Y. Liu, J.J. Zhao, X.L. Chen, V. Whoehling et al., Graphitic carbon nitride nanosheet electrode-based

high-performance ionic actuator. Nat. Commun. **6**, 7258 (2015)

30. X.J. Yan, X.Y. Wang, Y.Z. Dai, Y.Y. He, Z.B. Cai, Y. Wang et al., In situ self-assembly of SiO_2-coating Co_3O_4/graphene aerogel and its enhanced electrochemical performance for supercapacitors. J. Mater. Sci.: Mater. Electron. **30**, 17218–17226 (2019)

31. X.Y. Zhu, C. Yang, P.W. Wu, Z.Q. Ma, Y.Y. Shang, G.Z. Bai et al., Precise control of versatile microstructure and properties of graphene aerogel via freezing manipulation. Nanoscale **12**, 4882–4894 (2020)

32. M.A. Riaz, P. Hadi, I.H. Abidi, A. Tyagi, X.W. Ou, Z.T. Luo, Recyclable 3D graphene aerogel with bimodal pore structure for ultrafast and selective oil sorption from water. RSC Adv. **7**, 29722–29731 (2017)

33. X. Han, M. Kong, M.J. Li, X.K. Li, W.Q. Yang, C.X. Li, Nacre-based carbon nanomeshes for a soft ionic actuator with large and rapid deformation. J. Mater. Chem. C **8**, 1634–1641 (2020)

34. L.H. Lu, J.H. Liu, Y. Hu, Y.W. Zhang, W. Chen, Graphene-stabilized silver nanoparticle electrochemical electrode for actuator design. Adv. Mater. **25**, 1270–1274 (2013)

35. N. Terasawa, K. Asaka, Superior performance of PEDOT:poly(4-styrenesulfonate)/vapor-grown carbon fibre/ionic liquid actuators exhibiting synergistic effects. Sens. Actuators B **248**, 273–279 (2017)

36. D.M. Correia, J.C. Barbosa, C.M. Costa, P.M. Reis, J.M.S.S. Esperanca, V.D.Z. Bermudez et al., Ionic liquid cation size-dependent electromechanical response of ionic liquid/poly(vinylidene fluoride)-based soft actuators. J. Phys. Chem. C **123**, 12744–12752 (2019)

Publisher's Note Springer Nature remains neutral with regard to jurisdictional claims in published maps and institutional affiliations.